Available online at www.sciencedirect.com
ScienceDirect
Journal of the European Ceramic Society 27 (2007) 2917–2921
www.elsevier.com/locate/jeurceramsoc

Reflection intensity measurement using non-contact microwave probe and *in-plane* mappings for dielectric device

Hirofumi Kakemoto *, Jianyong Li, Takakiyo Harigai, Song-Min Nam, Satoshi Wada, Takaaki Tsurumi

Graduate School of Science and Engineering, Tokyo Institute of Technology, 2-12-1 Ookayama, Meguro, Tokyo 152-8552, Japan

Available online 24 January 2007

Abstract

The reflection intensity measurement using non-contact microwave probe was carried out for multi-layer ceramic capacitor. The spatial resolution of non-contact microwave probe was improved the basis of Kirchhoff's diffraction formula with decreasing diameters of the coaxial cable and probe. Using Reflection intensity mappings, the dielectric permittivity distribution in micro-region at 9.4 GHz was measured for the cross-section of a multi-layer ceramic capacitor at room temperature. The spatial resolution was experimentally estimated to be about 10 μm from mappings of the dielectric and inner electrode layers in the multi-layer ceramic capacitor.

Keywords: Microwave; MLCC

1. Introduction

Recently, ferroelectric and dielectric devices have been miniaturized. Particularly, multi-layer ceramic capacitors (MLCCs) have been prepared from $BaTiO_3$ (BT)-based material. In addition, further miniaturization and usage in high-frequency has been attempted for MLCCs, but the dielectric behavior in the local region of BT is not homogeneous, and has been reported as being functions of temperature, frequency and electric field. Therefore, high-frequency dielectric measurement on BT in a micro-region should be carried out. However, conventional dielectric measurement techniques are difficult for investigating the local dielectric properties at high-frequency region. Therefore, a high-frequency measurement method for the local dielectric properties should be developed.[1–3]

Recently, near-field scanning microwave microscopy has been developed by Steinhauer et al. using a λ/4 coaxial resonator and a contact probe, and local dielectric properties have been investigated with the contact probe scanning the surface of a sample at 7.2 GHz.[4,5]

On the other hand, a non-contact probe was used in this study to measure in a wide-frequency range and observe local dielectric properties; hence a microwave reflection (R) intensity was measured using the non-contact probe. The non-contact probe is useful for preventing resonance phenomena at a high-frequency, however, the impedance (Z) of a sample was found to be changed as a function of phase (θ) in an electric field incident for a sample. In a previous study, the accurate θ was adjusted for the measurement conditions, and dielectric permittivity was estimated with a non-contact state probe.[6]

In this study, we calculate the theoretical spatial resolution (SR): R intensity is measured using a non-contact probe up to 9 GHz, and *in-plane* R intensity mapping is carried out at the R intensity minimum position for a dielectric device (MLCC) owing to improved SR.

2. Experimental

Schematic illustrations of the measurement system and the transmission line considered as a model of the air-gap are shown in Fig. 1. The measurement system, as shown in Fig. 1(a), was constructed with an oscillator generated using a Gun diode, a phase (θ) shifter (0–360°), a directional coupler, a detector (diode), two types of coaxial cable and probes and XYZ stage. Table 1 shows the list of the coaxial cable and probe sizes.

The frequency (f) ranged from 8.5 to 11 GHz. The XYZ stage was moved by dc-servomotors (Chuo Precision Industrial Co., Ltd.), which were controlled by a personal computer using the

* Corresponding author. Tel.: +81 3 5734 2829; fax: +81 3 5734 2514.
E-mail address: hkakemot@ceram.titech.ac.jp (H. Kakemoto).

0955-2219/$ – see front matter © 2006 Elsevier Ltd. All rights reserved.
doi:10.1016/j.jeurceramsoc.2006.11.059

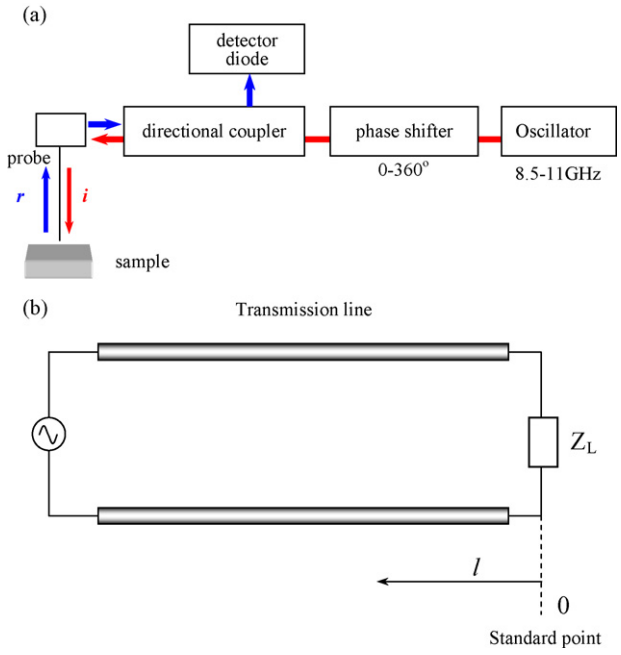

Fig. 1. Schematic illustrations of: (a) measurement system and (b) the transmission line considered as model for air-gap.

GP–IB interface. The air-gap that is the free space between the probe and the sample was considered as a transmission line, as shown in Fig. 1(b).

The samples were selected as a Cu-plate (size: 40 mm × 40 mm × 2.0 mm) and an MLCC (Murata electronics Co., Ltd., medium high voltage ceramic capacitor, size: 3.0 mm × 1.5 mm × 1.0 mm). The MLCC was cut perpendicular to its inner electrode (size: 1.0 mm × 1.5 mm × 1.0 mm), the cross-section of the MLCC was mirror like polished, and then the MLCC was put on the Cu-plate for measurement.

R intensity was measured at room temperature as a function of distance (*d*) between the probe and the sample. *In-plane* scanning was also carried out at the *R* intensity minimum point for the cross-section of MLCC (*yz*-plane)/Cu-plate.

3. Spatial resolution

Kirchhoff's diffraction formula was applied to an opening in an opaque screen and used for analysis to estimate SR. The oscillation of an electric field ($\Psi(r)$) at a position $r(x, y, z)$ is expressed as

$$\psi(r) = \frac{k}{4\pi \mathrm{i}} \int \rho \, \mathrm{d}\rho \int \exp(\mathrm{i}\theta) \, \mathrm{d}\theta \int \left[\frac{\exp(\mathrm{i}kr)}{r}\right] \mathrm{d}r, \quad (1)$$

where ρ is the radius, θ is the diffraction angle and k is the wavenumber.

Firstly, the intensity ($I(r) = |\Psi(r)|^2$) of the diffraction field based on Kirchhoff's diffraction formula was calculated using Eq. (1) as a function of *r*. In the integration of Eq. (1), the term of $\exp(\mathrm{i}kr)/r$ is difficult to integrate (Green's function). The integration of $\exp(\mathrm{i}kr)/r$ can be approximated as $\exp\{\mathrm{i}k(r - 1/r)\}\log r$. Secondly, *in-plane* intensity was also calculated using Eq. (1) as the functions of ρ and θ. The term of SR: $\lambda/\sin\alpha$ was inserted with exchanging the parameter during integration in Eq. (1). The normalized *in-plane* intensity is expressed by $I(\alpha)/I(0) = |\psi(\alpha)/\psi(0)|^2 = [bJ_1(A)^2] - aJ_1(A)^2]/A^2$, where, *a* and *b* are the radii of the probe and coaxial cable, respectively. J_1 is a Bessel function ($J_n(x)$, $n = 1$), α is the angle between the probe and the diffraction field and $A = (2\pi/\lambda)\sin\alpha$ (inverse SR), see Appendix A.

Fig. 2 shows the results of analysis for diffraction fields and *in-plane* intensities related to inverse SR, $(2\pi/\lambda)\sin\alpha$, using the above equations. From Fig. 2(b), the diffraction field is changed in the far-field, approximated as $\exp\{r^{-0.2}\}$ up to 10^{-3} m, near-field, approximated as $\exp\{r^{-0.22}\}$ from 10^{-5} to 10^{-3} m, and the proximity field, approximated as $\exp\{r^{-0.16}\}$, for less than 10^{-5} m with decreasing *r*. The measurements were done in the range from 5 to 0 mm, and as shown in Fig. 2(b), the measurement was hence carried out in the near-field.[7,8]

In Fig. 2(c and d), the minimum positions are seen at 6.17 m^{-1} for the test-probe, and at 11.54 m^{-1} for the micro-probe. From these results, the SRs of the test-probe and micro-probe were estimated to be 25.8 and 1.38 mm, respectively. The SR of the micro-probe was improved about 19 times in comparing with that of the test probe owing to decreasing diameters of the coaxial cable and probe.

4. Results and discussion

4.1. Reflection intensity measurement using probes

As shown in Fig. 1(b), the air-gap in measurement system was considered as the transmission line. The *R* intensity minimum was appeared owing to the inputting of the microwave into the sample, as a result of adjustment to $\theta = \pi/2$. The θ is denoted as $\theta = \beta l$, where β is $2\pi f/c$. If θ of a microwave incident on the sample is adjusted to $n\pi/2$, where *n* is an integer, *Z* presents the sample's one (Z_L). The microwave is transmitted to the sample. However, the *Z* of the sample at $\theta \neq n\pi/2$ increases and reflects the electromagnetic wave. Hence, it is important to measure *R* intensity with θ at $n\pi/2$ to estimate the dielectric permittivity (ε_r) of the sample.

Fig. 3 shows *R* intensity versus the distance (*d*) between the probe and the sample (Cu-plate) measured at 9.4 GHz using the test-probe (open triangles) and micro-probe (open circle). In both sets of *R* intensity data using the test-probe and

Table 1
Diameters for coaxial cables and probes, and lengths for probes.

Coaxial cable & Probe	Diameter & length	Remarks
Normal coaxial cable & test-probe	Coaxial cable: 3 mm ϕ, probe: 0.99 mm ϕ, probe length: 8 mm	–
Narrow coaxial cable & micro-probe	Coaxial cable: 1 mm ϕ probe: 0.3 mm ϕ, probe length: 4 mm	Probe top: 6 μm ϕ

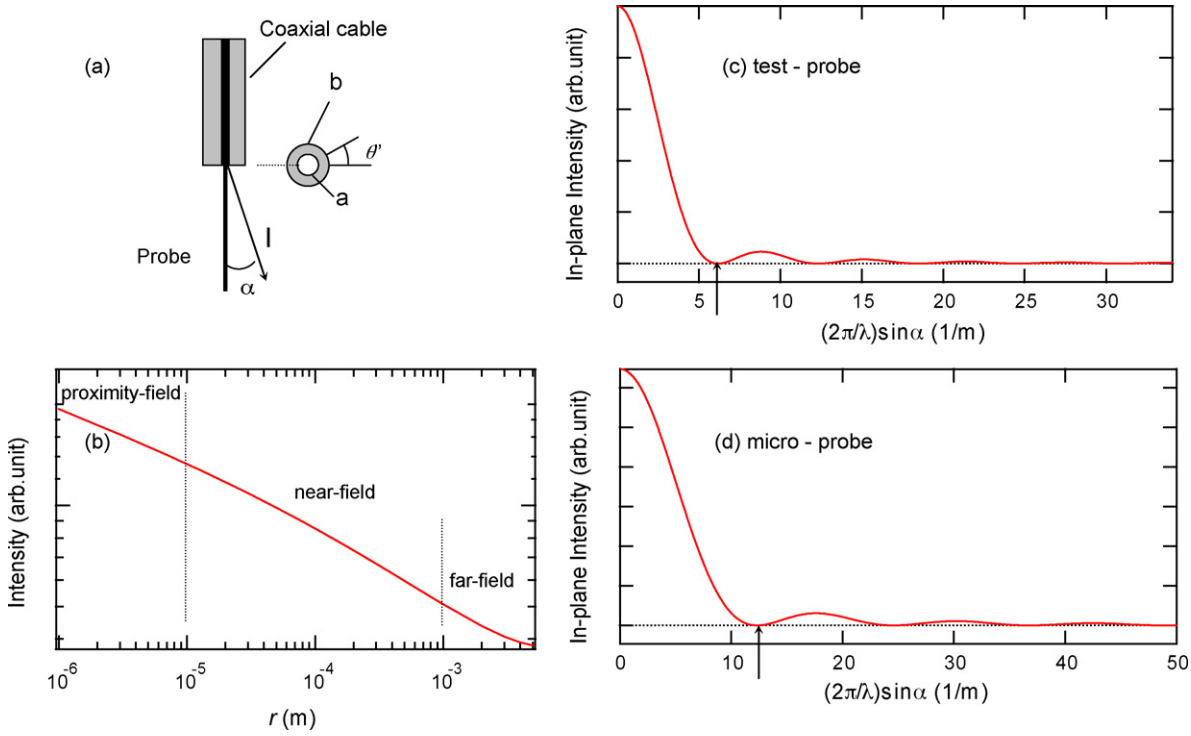

Fig. 2. (a) The dimension of coaxial cable and probe and calculated intensity based on Kirchhoff's diffraction formula, (b) diffraction intensity vs. distance between probe and sample, *in-plane* intensity vs. inverse spatial resolution (c) for test-probe and (d) for micro-probe.

micro-probe, R intensity minimum (R_{min}) appeared because the electromagnetic wave was inputting into the Cu-plate.

In chapter 3, the SR was, on the other hand, evaluated for coaxial cables and probes. The R intensity was decreased with a decreasing diameter of coaxial cable, as shown R intensity at $d = 5$ mm in Fig. 3. Therefore, to increase R intensity, as listed in Table 1, probe length of micro-probe was shortened.

As shown in Fig. 3, the R_{min} appeared at $d = 0.2$ mm for the test-probe and at $d = 0.1$ mm for the micro-probe, and the position of the R intensity minimum (d_{min}) for the micro-probe was shifted to a lower one because of shorten probe length. Although d_{min} was controlled by probe length, the R_{min} measured by the probes was however taken as the same value in Fig. 3. This is indicated that the R_{min} data exhibit that of Cu-plate itself. In addition, the shape of measured data using the micro-probe

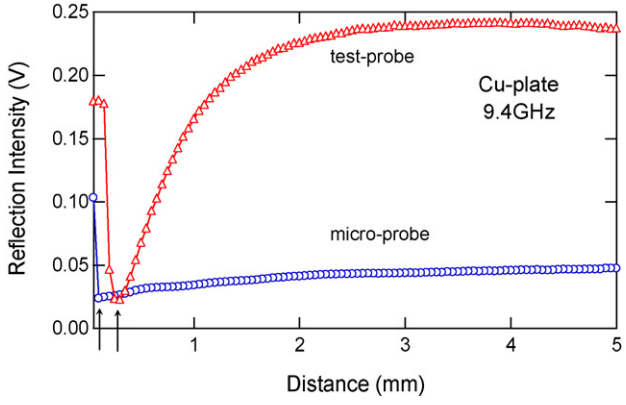

Fig. 3. Experimental reflection intensity vs. distance between probe and Cu-plate using test-probe and micro-probe at 9.4 GHz.

is similar to that calculated by the finite element time domain (FDTD) method in a previous study.[6]

To clarify R_{min}, consideration is taken of experimental data. The shapes of the measured data in Fig. 3 were changed at d_{min}. From $d = d_{min}$ to $d = 0$, R intensities were increased with decreasing d. These curves were caused by probe's properties. The Z of the probe (Z_{probe}) is given by $Z_{probe} = \exp\{-r^{-0.22}\}$ from the result of the calculation for the diffraction field, as shown in Fig. 2(b). From $d = 5$ mm to $d = R_{min}$, the air-gap can be considered as a transmission line, as shown in Fig. 1(b), as referred in the results of FDTD analysis in a previous report. Here, d is equivalent for electrical length (l). The Z of the transmission line (Z_{trans}) is expressed as $Z_{trans} = (Z_L + Z_o \tan \beta l)/(Z_o + Z_L \tan \beta l)$, where Z_o is characteristic Z. In this range, R intensity follows Z_{trans} property.[6]

The total impedance (Z_{tot}) of the measurement system is written as $Z_{tot} = Z_{probe} + Z_{trans}$, and the reflection coefficient ($\Gamma(l)$) is expressed as $\Gamma(l) = R/I = (Z_{tot} - Z_o)/(Z_{tot} + Z_o)$. Particularly, R_{min} is caused when $\theta = \beta l$ in Z_{trans} is equal to $\pi/2$ in R_{min} from curve fitting using the above equations.

4.2. Reflection intensity mappings using micro-probe

For *in-plane* R intensity mapping measurements, the micro-probe was used to improve SR at $d = (d_{min}) = 0.1$ mm. As the sample, the cross-section of the MLCC that was mirror like polished was used for the experimental determination of the SR and the micro-region dielectric behavior by observing the inner dielectric and electrode.

Fig. 4 shows the R intensity mappings for the cross-section of the MLCC using the micro-probe at R_{min} ($d = 0.1$ mm). In the

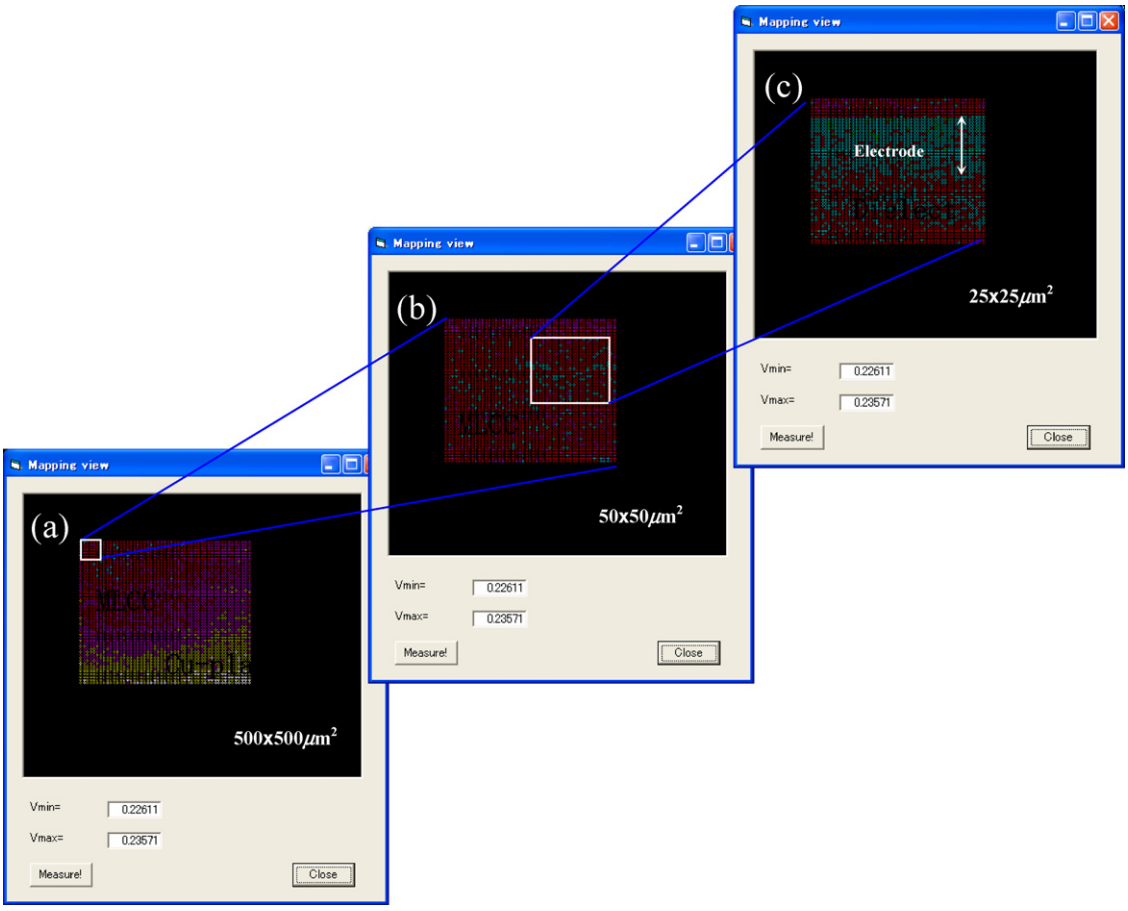

Fig. 4. Reflection intensity mappings: (a) 500μm × 500 μm, (b) 50μm × 50 μm and (c) 25μm × 25 μm for multi-layer ceramic capacitor measured at reflection intensity minimum position at 9.4 GHz.

upper region in Fig. 4(c), the inner electrode in the MLCC is clearly observed, and inner electrode's width is estimated to be about 10 μm in Fig. 4(c). The lower region in Fig. 4(c), however, showed the fraction of image because of the oscillator's stability. Although there are the fractions of image, the excellent improvement of the SR was realized by enhancing near-field using $d_{min} = 0.1$ mm in comparison with the theoretical analysis.

The ε_r could be transformed from obtained R intensity mappings, but the optical length (l_{opt}) is not in accordance with the samples that were used in a previous study, for example, Al_2O_3 (ALO) and $SrTiO_3$ (STO) single crystals. The optical length ($l_{opt} = \varepsilon_r^{0.5} l_o$) is changed as the functions of ε_r and sample length (l_o). In order to accordance with the optical length of, for example, Al_2O_3 ($\varepsilon_r = 10$, $x = 0.5$ mm, $l_{opt} = 1.58$ mm) and $SrTiO_3$ ($\varepsilon_r = 310$, $x = 0.5$ mm, $l_{opt} = 8.8$ mm) in ref. 6, l_o of the MLCC should be shortened in order to accordance with the l_{opt} of ALO and STO. The present l_{opt} of the MLCC in Fig. 4 is up to 63 mm (=$4000^{0.5} \times 1.0$), but the transformation of ε_r will be carried out in a future study.[4–6,9,10]

5. Conclusions

In this study, the spatial resolution and the mechanism of the appearance of the reflection intensity minimum were elucidated, and *in-plane* reflection intensity mappings using a non-contact microwave probe was carried out using the improved measurement condition.

The spatial resolution was improved the basis of Kirchhoff's diffraction formula by decreasing the diameters of the coaxial cable and probe. The reflection intensity minimum was caused by input microwave into the sample as the results of phase equal to $\pi/2$.

From the reflection intensity mappings at the reflection intensity minimum position, the dielectric permittivity distribution in the micro-region at 9.4 GHz was measured for the cross-section of a multi-layer ceramic capacitor. The spatial resolution was experimentally estimated to be at least 10 μm from the mappings of the inner dielectric and electrode layers in the multi-layer ceramic capacitor.

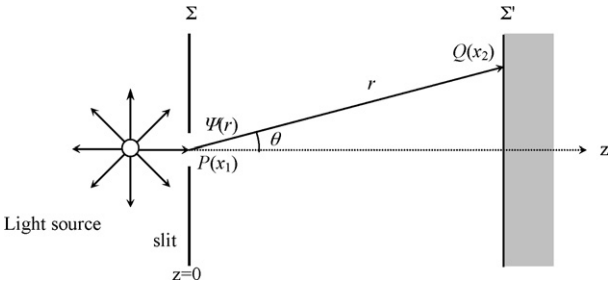

Fig. A.1. The diffraction from slit to opaque screen.

Acknowledgments

The author would like to thank Murata Electronic Ltd. for supplying the multi-layer ceramic capacitor (GRM31A703A100JW31D). This work was supported by the Japan Society Promotion for the Science (Project No. 16760542).

Appendix A

The oscillation of the electric field ($\Psi(r)$) at $r(x, y, z)$ is defined as

$$\psi(r) = \frac{k}{4\pi \mathrm{i}} \int \rho \, \mathrm{d}\rho \int \exp(\mathrm{i}\theta) \, \mathrm{d}\theta \int \left[\frac{\exp(\mathrm{i}kr)}{r}\right] \mathrm{d}r, \qquad (A.1)$$

where ρ is the radius of a slit, θ the diffraction angle, and r is the position (PQ). The light source, slit (Σ), and an opaque screen (Σ') are positioned as shown in Fig. A.1.

The points P and Q are positioned at x_1 and x_2, respectively. The r is defined as $r = [(x_2 - x_1)^2 + z^2]^{0.5}$, and is approximated to be $z[1 + (x_2 - x_1)/z]^{0.5} = z - x_1x_2/z$. The term of $\exp(\mathrm{i}kr)/r$ is difficult to integrate (Green function).

A.1. Integration as a function of r

In the case of $r \ll \lambda$ (=32 mm, f = 9.4 GHz), the Eq. (A.1) is transformed to $\psi(r) = \int u_0[\exp\{\mathrm{i}k(z - x_1x_2/z)\}/z] \, \mathrm{d}z$, and it is equivalent to $\int u_0[\exp(\mathrm{i}kz)/z]\exp\{\mathrm{i}k(-x_2x_1/z)\} \, \mathrm{d}z$. Then, this function is integrated to be $\Psi(r) = \exp[\mathrm{i}k(z - 1/z)]\log x$. The integrated function is rewritten as $\Psi(r) = \exp[\mathrm{i}k(r - 1/r)]\log r$.

A.2. In-plane integration

In-plane term of Eq. (A.1) is $\psi(\rho, \theta)) = \int_a^b \rho \, \mathrm{d}\rho \int_0^{2\pi} \exp(\mathrm{i}\theta) \, \mathrm{d}\theta$. Where the spatial resolution term is expressed as $\lambda/\sin\alpha$, spatial resolution are inserted with exchanged the parameter in integration, and this function can be integrated to be $\psi(\alpha) = 2\pi \int_0^{2\pi} \rho J_o((2\pi\rho/\lambda)\sin\alpha) \, \mathrm{d}\rho = (1/A)bJ_1(bA) - (1/A)aJ_1(aA)$, where A is the inverse spatial resolution $(2\pi/\lambda)\sin\alpha$.

References

1. Moulson, A. J. and Herbert, J. M., *Electroceramics, Properties, Applications* (*1st ed.*). Chapman & Hall, New York, 1990, p. 74.
2. Afsar, M. N., Birch, J. R. and Clarke, P. N., *Proc. IEEE*, 1986, **74**, 183.
3. Kakemoto, H., Li, J., Nam, S.-M., Wada, S. and Tsurumi, T., *Jpn. J. Appl. Phys.*, 2003, **42**, 6143.
4. Steinhauer, D. E., Vlahacos, C. P., Wellstood, F. C., Anlage, S. M., Canedy, C., Ramesh, R., Stanishevsky, A. and Melngailis, L., *Appl. Phys. Lett.*, 1999, **75**, 3180.
5. Steinhauer, D. E., Vlahacos, C. P., Wellstood, F. C., Anlage, S. M., Canedy, C., Ramesh, R., Stanishevsky, A. and Melngailis, J., *Rev. Sci. Instrum.*, 2000, **71**, 2751.
6. Kakemoto, H., Nam, S.-M., Wada, S. and Tsurumi, T., *Jpn. J. Appl. Phys.*, 2006, **45**, 3002.
7. Düring, U., Pohl, D. W. and Rohner, F., *J. Appl. Phys.*, 1986, **59**, 3318.
8. Ootsu, M. and Kobayashi, K., *Kinsetsuba-ko no Kiso*. Ohmsha, Tokyo, 2003, p. 16 [in Japanese].
9. Ash, E. A. and Nicholls, G., *Nature*, 1972, **237**, 510.
10. Wei, T., Xiang, X.-D., Wallace-Freedman, W. G. and Schultz, P. G., *Appl. Phys. Lett.*, 1996, **68**, 3506.